NUMERICAL STUDY OF THE EFFECTS OF CROSS-WIND ON THE JET BLAST DEFORMATION

Keiichi Ishiko*, Atsushi Hashimoto*, Yuichi Matsuo*, Shigeya Watanabe*
*** Japan Aerospace Exploration Agency**
ishiko@chofu.jaxa.jp

Keywords: *CFD, Jet blast, Cross-wind*

Abstract

In Tokyo international airport (Haneda airport), runways A and B have a cross over point shown in Fig. 1. At this point, it may be possible that the jet blast of aircraft on takeoff from the runway A constitutes a hazard for another aircraft landing on the runway B. For operational safety and for improvement of capacity and efficiency of air traffic control, it is required to predict the trajectory of long-distance jet blast with high accuracy. In order to examine far-field velocity of jet blast by computational fluid dynamics (CFD), simulation using Reynolds averaged Navier-Stokes (RANS) equation is carried out with very large computational domain in this research. The velocity profiles obtained by numerical simulation agree well with those obtained by experiments. Then, we perform the parametric study of wind direction. It is found that the wind direction angle that has more effect on the deflection of jet blast is lower than ninety degrees. Moreover, the trajectory of jet blast can be described by power law.

1 Introduction

Airports which have a large amount of transportation have problem of capacity and efficiency of air traffic control (ATC). Currently, the wake turbulence as like vortices from wing tip is main factor for the problem. Recently, however, it becomes important to consider a plume of hot and high velocity gas emitted from the exhaust of a jet engine particularly on or before takeoff with increase of usage of airport. This exhaust of jet is called as jet blast. In Tokyo international airport (Haneda airport), runways A and B have a cross over point shown in Fig. 1. At this point, it may be possible that the jet blast of aircraft on takeoff from the runway A constitutes a hazard for another aircraft landing on the runway B. For operational safety and for improvement of capacity and efficiency of air traffic control (ATC), it is required to predict the trajectory of long-distance jet blast with high accuracy up to far-field.

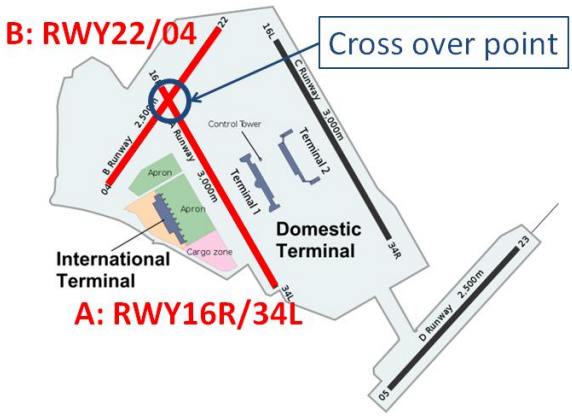

Fig. 1 Tokyo international airport (Haneda airport).

Khritov et al. has investigated on the far-field velocity of wall jets in experiments and numerical simulations.[1] In their paper, it is described about a behavior of jet, a development of turbulence and a influence of buoyancy for hot jet, comparing with the data obtained by other researchers. However, there are not so many researchers on the behavior of long-distance jet compared with those focused near the nozzle exit. Moreover, there are few researches about cross-wind effect.[2,3]

Therefore, it is not enough to understand the actual phenomena as is common in airport.

On the other hand, in Japan, Ministry of Land, Infrastructure, Transport and Tourism (MILT) performed far-field velocity measurements of jet blast from Boeing 777-300 anchored on the runway of Haneda airport in March 2010. However, the measurement area was restricted and the obtained data was discrete and coarse. Moreover, the flow was affected by strong cross-wind. In order to examine the influence of cross-wind and to understand the actual phenomena of jet blast in airport, the numerical analysis by computational fluid dynamics (CFD) has been expected.

The purpose of this study is to clarify the phenomena of jet blast to predict the trajectory of long-distance jet blast in Haneda airport with high accuracy by CFD. To achieve this purpose, very large computational domain, at least few hundred times of jet nozzle diameter on a side. In this study, we perform numerical simulations of the blast from two coaxial jets by using the Reynolds averaged Navier-Stokes (RANS) equation with very large computational domain. We compare the obtained far-field velocity with that obtained by experiments. In comparison of results obtained by numerical simulations, the sensitivity of strength of cross-wind is examined briefly. Moreover, we perform parametric study to investigate the dependency of cross-wind direction.

2 Numerical Methods

2.1 Fast CFD solver

As an unstructured flow solver, a newly-developed fast CFD solver called FaSTAR (FaST Aerodynamic Routines)[4] is used. The governing equations for the three-dimensional viscous compressible flow are given by the Reynolds averaged Navier-Stokes equations. These equations are solved on the unstructured grid by a cell-centered finite volume method. Because a broad Mach number flow appears in the interested flowfield, in order to evaluate the numerical flux functions, we employ a simple low-dissipation AUSM (SLAU)[5] which ahs smaller numerical viscosity not only for high speed region but also for low speed region. The second-order spatial accuracy is realized by a linear reconstruction of primitive variables with Green-Gauss method and Venkatakrishnan like limiter extended for unstructured grid is used. For time integration, LU-SGS (Lower/Upper Symmetric Gauss-Seidel) implicit method[6] is used. As for turbulence model, SST (Shear Stress Transport) turbulence model[7,8] is used. The equations for the turbulence model are also solved using the second-order scheme.

2.2 Shear Stress Transport (SST) Turbulence Model

The shear stress transport (SST) turbulence model is one of two-equation models and there are some versions of this model. The formulation after 2003 is used in this study that is given by

$$\frac{\partial \rho k}{\partial t}+\frac{\partial \rho u_j k}{\partial x_j}=P-\beta^* \rho \omega k + \frac{\partial}{\partial x_j}\left[(\mu+\sigma_k \mu_t)\frac{\partial k}{\partial x_j}\right], \tag{1}$$

$$\frac{\partial \rho \omega}{\partial t}+\frac{\partial \rho u_j \omega}{\partial x_j}=\frac{\gamma}{\nu_t}P-\beta \rho \omega^2 + \frac{\partial}{\partial x_j}\left[(\mu+\sigma_\omega \mu_t)\frac{\partial \omega}{\partial x_j}\right] + 2(1-F_1)\frac{\rho \sigma_{\omega 2}}{\omega}\frac{\partial k}{\partial x_j}\frac{\partial \omega}{\partial x_j}, \tag{2}$$

where γ, β, σ_k and σ_ω denote the model coefficients. These model coefficients is given by two sets of parameters as shown in Table 1, which are the constants for inner part of the boundary layer denoted by subscript 1 and those for outer part of the boundary layer denoted by subscript 2. Then they are combine by using blending function F_1.

$$\phi = F_1\phi_1 + (1-F_1)\phi_2 . \quad (\phi = \gamma, \beta, \sigma_k, \sigma_\omega) \tag{3}$$

Tab. 1 The model coefficients for SST-2003.

Inner boundary	Outer boundary
$\gamma_1 = \frac{5}{9}$	$\gamma_2 = 0.44$
$\beta_1 = 0.075$	$\beta_2 = 0.0828$
$\sigma_{k1} = 0.85$	$\sigma_{k2} = 1.0$
$\sigma_{\omega 1} = 0.5$	$\sigma_{\omega 2} = 0.856$

3 Comparisons with Experiments

3.1 Measured Velocity Data

For the far-field velocity measurements of jet blast from Boeing 777-300, the fifty-four anemometers were installed on five lines located downstream side of the nozzle exits, which were at about $200D_{core}$, $300D_{core}$, $405D_{core}$, $500D_{core}$ and $600D_{core}$, where D_{core} denotes the core nozzle diameter. The configurations of anemometers are illustrated in Fig. 2. In the measurements, the condition of engine pressure ratio (EPR) was 1.186 and this value is large sufficiently.

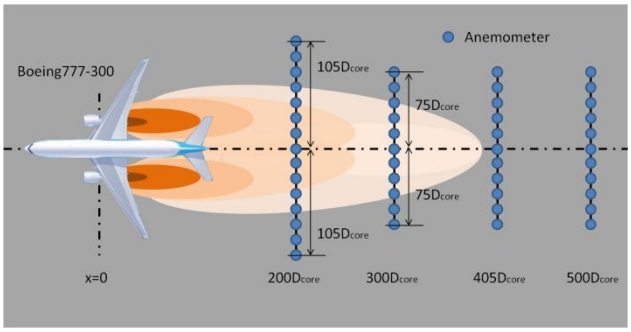

Fig. 2 Configuration of anemometers in measurements.

In measurements, the strong cross-wind swept the jet blast out of measurement area. Especially, anemometers located at more than $405D_{core}$ from nozzle exits could measure only cross-wind. The magnitude of the cross-wind was about 3.5 m/sec and the estimated velocity components of cross-wind were about $u_{wind} = -1.59$ [m/sec] in the direction from nose to tail and about $w_{wind} = 3.12$ [m/sec] in the direction from right to left, respectively.

3.2 Brief Descriptions for Computation

The Boeing 777-300 has turbofan engines which have $2D_{core}$ diameter of fan nozzle. In order to simulate the jet blasts from Boeing 777-300, the coaxial jets from two cylindrical nozzles are considered. The schematic view of the computational domain is illustrated in Fig. 3. The computational domain is about $30D_{core}$ in upstream side and $L_x = 500D_{core}$ in downstream side of the nozzle exit and $L_y = 200D_{core}$ in the normal direction to the wall surface. In spanwise direction, the domain is $L_{zr} = 100D_{core}$ in right hand side of the jets and $L_{zl} = 500D_{core}$ in left hand side. The whole computational grid is shown in Fig. 4. The total number of computational grid is about 22 millions. The length of nozzles is about $30D_{core}$. Figure 5 shows the close up view of the computational grid around the nozzle exits. The red region denotes the inflow of core nozzle flow and the yellow that of fan nozzle flow. The center axis of the jets are located at the height of $3D_{core}$ and the distance between two jet centers is $19D_{core}$.

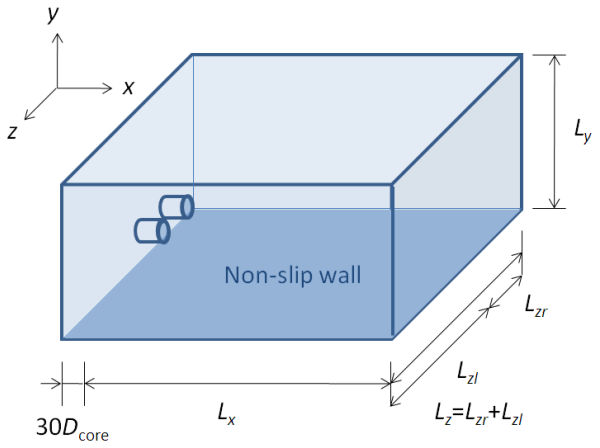

Fig. 3 Schematic view of computational domain.

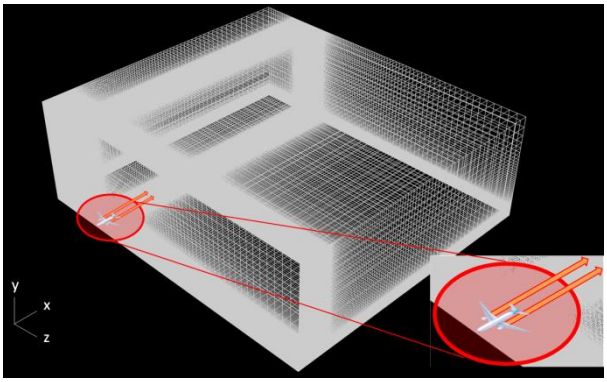

Fig. 4 Computational grid in entire region.

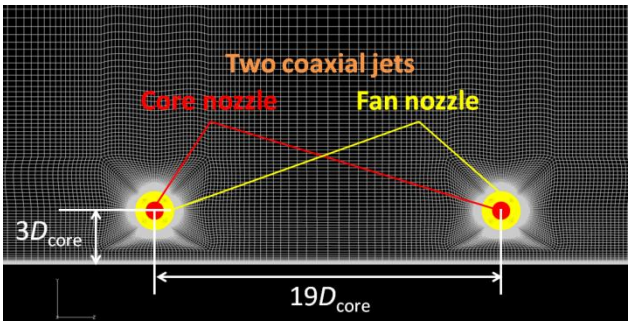

Fig. 5 Computational grid around the nozzle exits.

The inflow conditions from the core and the fan nozzles are given by the results from estimation of turbofan engine performance. At the condition that engine pressure ratio is 1.186, the obtained inlet Mach numbers are $M_{core} = u_{core} / a_{core} = 0.51$ for core nozzle flow and $M_{fan} = u_{fan} / a_{fan} = 0.70$ for fan nozzle flow, respectively. The reason of lower Mach number of core nozzle flow than that of fan nozzle flow is that the sound of speed is faster than that of fan nozzle flow due to high temperature of core nozzle flow. We assume that the optimum expansion at the nozzle exit is achieved for both core and fan nozzle.

We assume the non-slip adiabatic wall condition on the ground surface. On the surface of side wall of coaxial nozzles, slip wall condition is assumed. The ratio of specific heat and universal gas constant are set as $\gamma = 1.4$ and $R = 287$ J kg^{-1}K^{-1}, respectively. The laminar and turbulent Prandtl numbers are assumed as 0.71 and 0.9, respectively.

3.3 Results and Discussions

In order to compare the results obtained by measurements and to examine the sensitivity of measured cross-wind, we perform computations with two different wind velocities which are SST and SST-small shown in Table 2. The velocity components in spanwise direction are $w_{wind} = 3.12$ m/sec in SST and $w_{wind} = 1.76$ m/sec in SST-small, respectively. For both cases, the velocity component in streamwise direction is $u_{wind} = -1.59$ m/sec. The magnitude of wind velocities for SST and SST-small are $U_{sst} = 3.50$ m/sec and $U_{SST-small} = 2.37$ m/sec, respectively. The cross-wind velocity of condition in SST is the same with that obtained in measurements. In the obtained results, velocity is normalized by thrust-equivalent-velocity which is defined as follows:

$$U_{thrust}^2 = \frac{T}{\rho_\infty A_{total}} = \frac{2\pi \int_0^{r_{fan}} \rho U^2 r dr}{\pi r_{fan}^2 \rho_\infty}, \qquad (4)$$

where T denotes the thrust, A_{total} the total area of core and fan nozzles, ρ_∞ the ambient density, r_{fan} the radius of fan nozzle, respectively. The density ρ and the velocity U of the nozzle flow are function of the radial distance r. In this study, value of the thrust-equivalent-velocity is $U_{thrust} = 222.13$ m/sec.

Tab. 2 Computation cases associated with comparison with experiments.

Case	u_{wind}, m/sec	w_{wind}, m/sec
SST	–1.59	3.12
SST-small	–1.59	1.76

Figure 6 shows the comparison of the magnitude of velocity at (a) $x/D_{core} = 200$, $y/D_{core} = 1.5$, and at (b) $x/D_{core} = 300$, $y/D_{core} = 3.0$. In this figure, both the order of magnitude and the location of peak obtained by SST agree quite well with those of experiments. On the other hand, it is found that the location

of peak obtained by SST-small is different from the others. This indicates that the sensitivity of cross-wind is very large because the difference of cross-wind velocity between SST and SST-small is very small against the thrust-equivalent-velocity that is given by

$$\frac{|U_{SST} - U_{SST-small}|}{U_{thrust}} \approx 5.09 \times 10^{-3} \qquad (5)$$

.

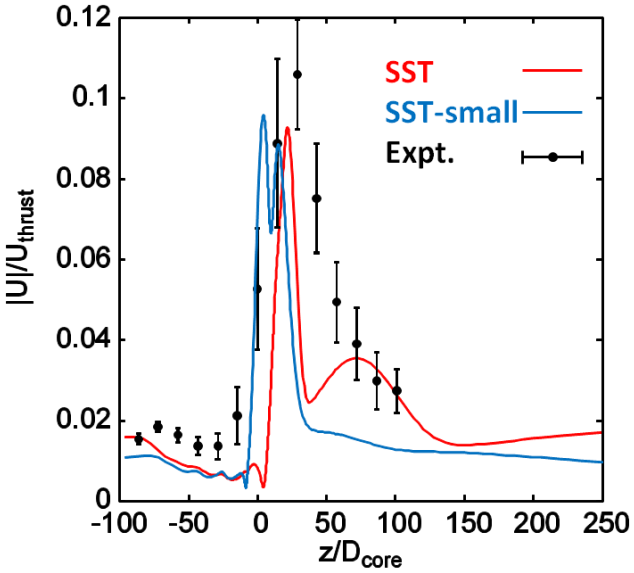

(a) $x/D_{core} = 200$, $y/D_{core} = 1.5$.

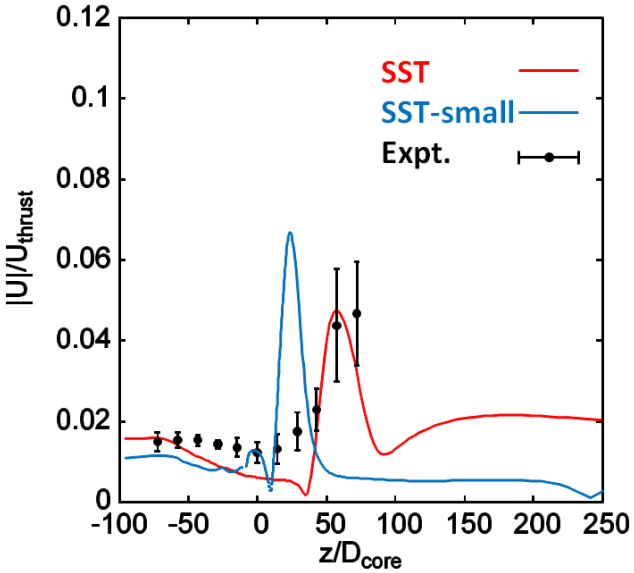

(b) $x/D_{core} = 300$, $y/D_{core} = 3.0$.

Fig. 6 Comparison of the magnitude of velocity profiles obtained in SST and SST-small comparing with experimental data.

It is also found that the local minimal values appear in the velocity profiles obtained by numerical simulation, however, those minimal value does not appear in the experiments. One of the possible reasons of that is turbulence model. In order to specify the reason, a detailed examination of the applicability of turbulence model should be carried out by comparing with fundamental experiments.

4 Parametric Study of Cross-Wind Direction angles

4.1 Brief Descriptions for Computation

In this section, the coaxial jets from two cylindrical nozzles are considered. The inflow inlet Mach numbers are $M_{core} = 0.51$ for core nozzle flow and $M_{fan} = 0.70$ for fan nozzle flow, respectively. We assume the non-slip adiabatic wall condition on the ground surface. On the surface of side wall of coaxial nozzles, slip wall condition is assumed. The laminar and turbulent Prandtl numbers are assumed as 0.71 and 0.9, respectively. The computational domain is about $30D_{core}$ in upstream side and $L_x = 1000D_{core}$ in downstream side of the nozzle exit and $L_y = 500D_{core}$ in the normal direction to the wall surface. In spanwise direction, the domain is $L_{zr} = 200D_{core}$ in right hand side of the jets and $L_{zl} = 1000D_{core}$ in left hand side. The total number of computational grid is about 26 millions. The length of nozzles is about $30D_{core}$. The centers of jet are located at $3D_{core}$ from the non-slip surface. The ratio of specific heat and universal gas constant are set as $\gamma = 1.4$ and $R = 287$ J kg^{-1}K^{-1}, respectively.

The magnitude of cross-wind is set to 3.5 m/sec. Figure 7 shows the definition of wind direction angle θ. The seven computations of different wind directions are carried out, which are 30, 45, 60, 75, 90, 120 and 150 degrees, respectively. The velocity components of each case are summarized in Table 3.

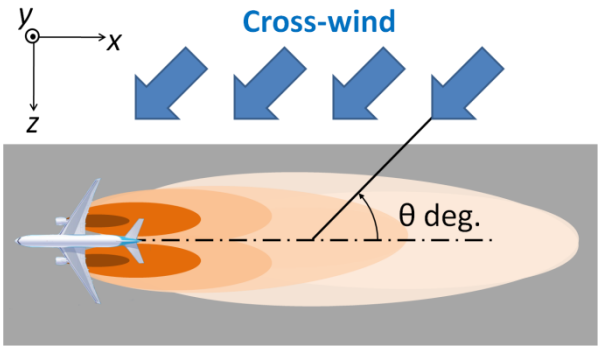

Fig. 7 Definition of cross-wind direction angle.

Tab. 3 Computation cases for parametric study of wind direction.

Wind direction θ, deg.	$\lvert U_{wind} \rvert$, m/sec	u_{wind}, m/sec	w_{wind}, m/sec
30	3.5	–3.03	1.75
45	3.5	–2.47	2.47
60	3.5	–1.75	3.03
75	3.5	–0.91	3.38
90	3.5	0.00	3.50
120	3.5	1.75	3.03
150	3.5	3.03	1.75

4.2 Results and Discussions

In order to compare the behavior of jet blast, obtained contours of $|U|/U_{thrust}$ in the plane parallel to the wall at $y/D_{core} = 3.0$ are shown in Fig. 8. As can be seen in Fig 8, the cross-wind sweeps the jet blast and pushes back for the cases of smaller wind direction angle than ninety degrees. On the other hand, jet blast is stretched in the direction of jet axis for the cases of larger wind direction angle than ninety degrees.

Figure 9 shows the typical obtained velocity profiles at several downstream locations in the plane parallel to the wall at $y/D_{core} = 3.0$. In Fig. 9, the midpoint of two coaxial jet centers is located at $z/D_{core} = 0$. From this figure, deflection distance is defined as the spanwise location z_{peak} that gives peak velocity $|U|_{peak}$. In order to examine the behavior of jet blast, the deflection distance and peak velocity are plotted against the wind direction angle θ in Fig. 10 and 11, respectively. In these figures, for cases of $\theta > 90$, the deflection distance decreases and peak velocity increases monotonically, respectively, with increasing wind direction angle θ. On the other hand, for cases of $\theta < 90$, they become a little more complicated than that of $\theta > 90$. In Fig. 10, it is found that the minimum value of $|U|_{peak}/U_{thrust}$ appears between $\theta = 45$ and 90 degrees. In Fig. 11, it is seen that a maximum value of z_{peak}/D_{core} is given by $\theta = 60$ or 75 degrees. Figure 12 shows the schematic view of the effect of cross-wind on jet blast. The jet blast is the most affected at the location where the wind velocity component normal to flow path of jet blast becomes largest, here after we refer to such location as maximum contribution point. For $\theta > 90$, the maximum contribution point always appears at nozzle exit. The tangential component of corss-wind to jet blast becomes larger and the normal component becomes smaller with increasing wind direction angle, respectively. Therefore, the contribution of cross-wind decreases as the angle increases. For $\theta < 90$, the maximum contribution point appears somewhere on the flow path of jet blast. This point shifts toward upstream side of the jet blast up to nozzle exit with increasing the wind direction angle. However, the momentum of jet blast reaches maximum at the nozzle exit. The jet blast is hard to be deflected when the momentum of jet blast is large at the maximum contribution point. This is reason why behaviors of the deflection distance and peak velocity become a little more complicated for cases of $\theta < 90$ than that for the cases of $\theta > 90$

Figure 13 shows the trace of the path of peak velocity $|U|_{peak}/U_{thrust}$ on the plane parallel to the wall at $y/D_{core} = 3.0$, which corresponds to the trajectory of the jet blast. In the figure, plotted symbols are CFD results and solid lines are least squares fitting curves on the log-log scale. As can be seen from this figure, the trajectory of jet can be described by power law, $z/D_{core} = \alpha(x/D_{core})^n$, where n denotes the power index and α the coefficient. The obtained power index n shows about three for all cases of wind direction, and they are summarized in Table 4. However, it seems that the power index depends on the wind direction,

the momentum of jet and the atmospheric boundary layer, and so on, which needs further investigation.

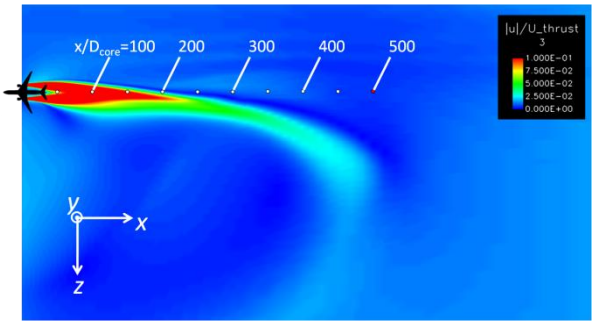

(a) 30 deg.

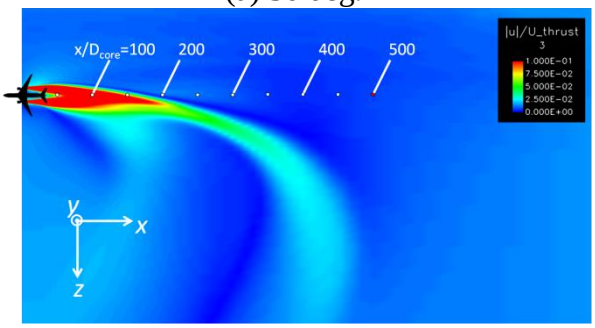

(b) 45 deg.

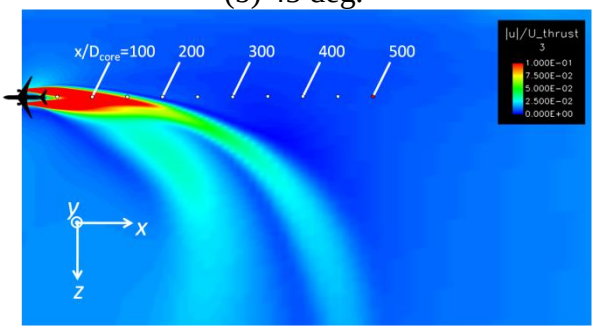

(c) 60 deg.

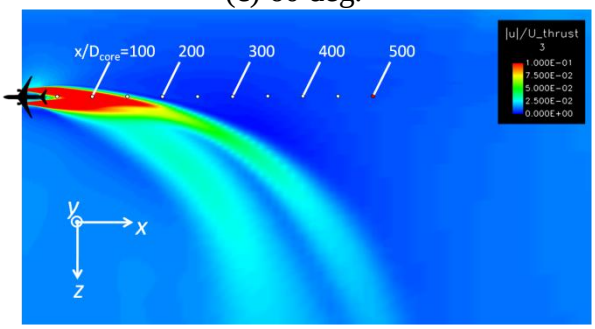

(d) 75 deg.

Fig. 8 Obtained contours of $|U|/U_{thrust}$ in the plane parallel to the wall at $y/D_{core} = 3.0$.

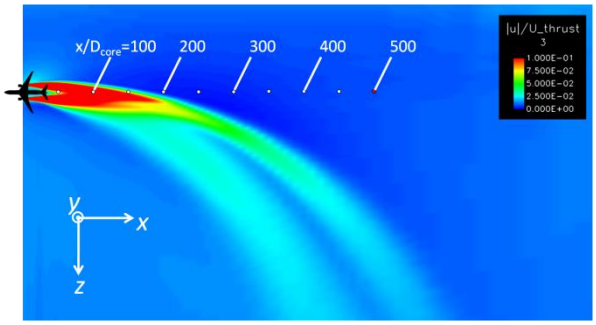

(e) 90 deg.

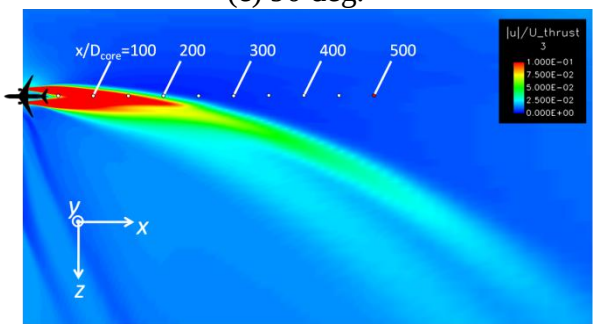

(f) 120 deg.

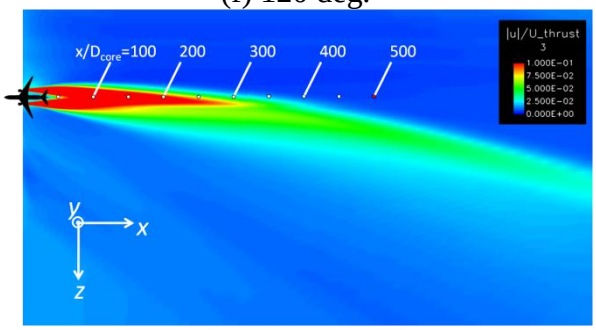

(g) 150 deg.

Fig. 8 Contd.

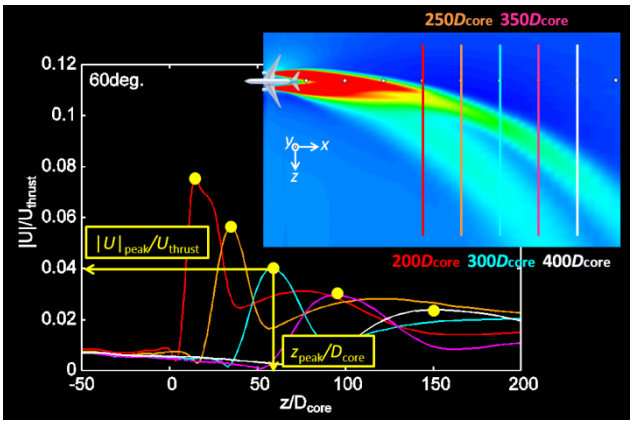

Fig. 9 Obtained $|U|/U_{thrust}$ profiles at each downstream location at $y/D_{core} = 3.0$ and definition of peak velocity $|U|_{peak}$ and deflection distance z_{peak}.

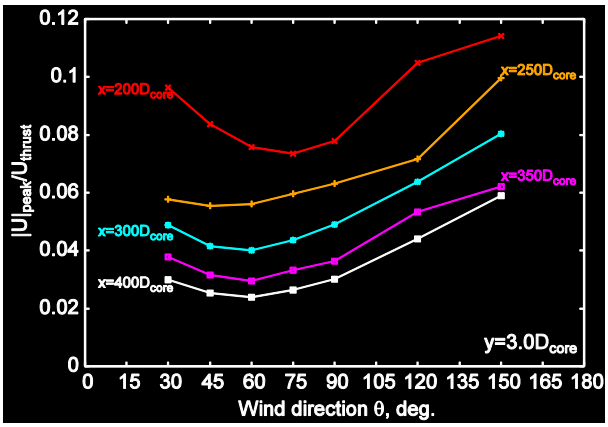

Fig. 10 Distributions of peak velocity $|U|_{peak}/U_{thrust}$.

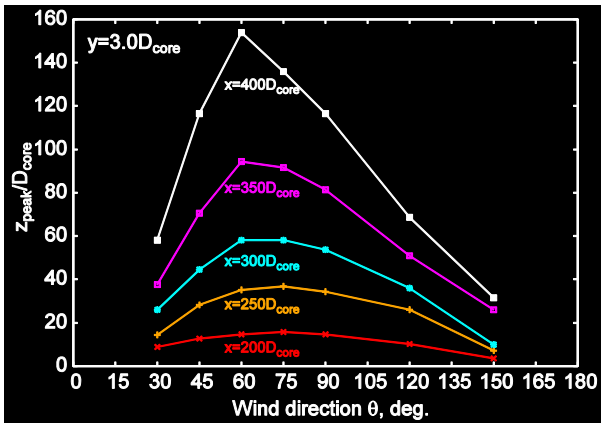

Fig. 11 Distributions of spanwise location giving peak velocity.

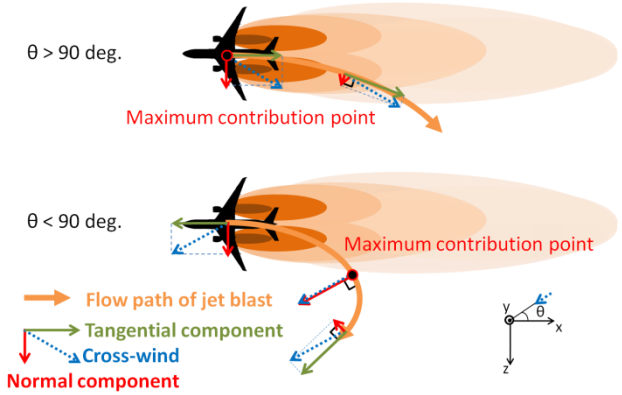

Fig. 12 Schematic view of the effect of the cross-wind on jet blast.

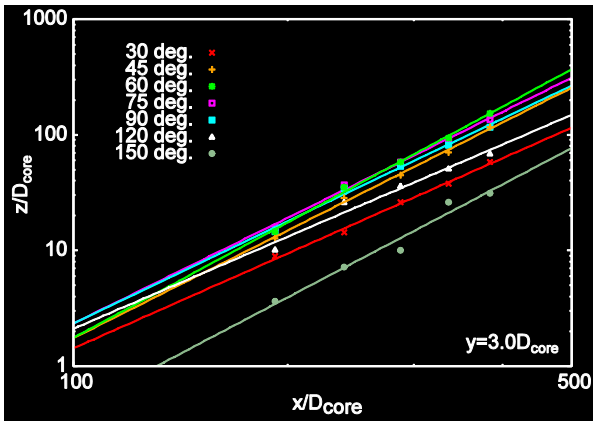

Fig. 13 Trace of the path of peak velocity $|U|_{peak}/U_{thrust}$ on the plane parallel to the wall at $y/D_{core}=3.0$ plotted in log-log scale. The solid line indicates power law.

Tab. 4 Obtained coefficients of power law fit, $z/D_{core}=\alpha\left(x/D_{core}\right)^{n}$, in Fig. 13.

Wind direction θ, deg.	α	n	R^2
30	4.94×10^{-6}	2.73	0.995
45	1.12×10^{-6}	3.10	0.996
60	4.04×10^{-7}	3.32	0.996
75	1.97×10^{-6}	3.04	0.995
90	3.11×10^{-6}	2.94	0.991
120	1.08×10^{-5}	2.65	0.967
150	1.40×10^{-7}	3.24	0.967

5 Conclusions

In this study, the steady state of two coaxial jets with cross-wind were computed by using very large computational domain, in order to predict the jet blast from the engines of Boeing 777-300. The peak location and the order of value of velocity obtained by numerical simulations agreed well with those obtained by experiments. It was found that the sensitivity of strength of cross-wind was very large.

Then, the parametric study of cross-wind direction was carried out. It was found that the wind direction angle that had more effect on the deflection of jet blast was lower than ninety degrees. Moreover, the trajectory of jet blast could be described by power law and the obtained power index was $n\approx3$ for all cases in the present computations. However, further

investigation is necessary due to the influence of wind direction, momentum of jet and atmospheric boundary layer.

On the other hand, the shape of velocity profiles obtained by numerical simulations was partially different from those obtained by experiments. This may be because of turbulence model. Therefore, a detailed examination of applicability of turbulence model should be carried out by comparing with fundamental experiments and it is our future works.

Acknowledgement

The velocity data of jet blast for Boeing 777-300 measured at Tokyo international airport (Haneda airport) in March 2010 was provided by ministry of Land, Infrastructure, Transport and Tourism (MILT). The turbofan engine performance data was prepared by Mr. Hisao Futamura of Clean Engine Team, Aerospace Research and Development Directorate in JAXA. Computations were carried out on Fujitsu FX1 at JAXA Supercomputer System.

References

[1] Khritov, K.M., Lyubimov, D.A., Maslov, V.P., Mineev, B.I., Secundov, A.N. and Birch, S.F., "Three-Dimensional Wall Jets: Experiment, Theory and Applicatoin," AIAA paper 2002-0723, 2002.

[2] Lee, J., Birch, S.F. and Scovill, B.A., "Airport jet plume zone mapping," *Journal of Aircraft*, Vol. 33, No. 4, pp. 737-742, 1996.

[3] Keffer, J.F. and Baines, W.D., "The round turbulent jet in a cross-wind," *Journal of Fluid Mechanics*, Vol. 15, No. 4, pp. 481-497, 1963.

[4] Watanabe, S., Kuchi-ishi, S., and Aoyama, T., "A prototype system towards EFD/CFD integration: Digital/analog-hybrid wind tunnel," *Proceedings of the 27th International Congress of the Aeronautical Sciences ICAS*, 2010.

[5] Shima, E., Keiichi, K., "On new simple low-dissipation scheme of AUSM-family for all speeds," AIAA paper2009-136, 2009.

[6] Sharov, D. and Nakahashi, K., "Reordering of hybrid unstructured grids for lower-upper symmetric Gauss-Seidel computations," AIAA Journal, Vol. 36, No. 3, pp. 484-486, 1998.

[7] Wilcox, D.C., *Turbulence Modeling for CFD*, DCW Industries, Inc., 2nd edition, 1994.

[8] Menter, F.R., Kuntz, M. and Langtry, R., "Ten years of industrial experience with the SST turbulence model," *Turbulence, Heat and Mass Transfer*, ed: Hanjalic, K., Nagano, Y. and Tummers, M., Inc., pp. 625-632, 2003.

Copyright Statement